

Application of convex cone analysis to hyper-spectral and multi-spectral scenes

John Gruninger^{*}, Jamine Lee and Robert Sundberg
Spectral Sciences, Inc., 99 S. Bedford St, Burlington, MA 01803

ABSTRACT

A new end-member analysis method based on convex cones has been developed. The method finds extreme points in a convex set. Unlike convex methods that rely on a simplex, the number of end-members is not restricted by the number of spectral channels. The algorithm simultaneously finds fractional abundance maps. The fractional abundances are the fractions of the total spectrally integrated radiance of a pixel that are contributed by the end-members. A physical model of the hyper-spectral or multi-spectral scene is obtained by combining subsets of the end-members into bundles of spectra for each scene material. The bundle spectra represent the spectral variability of the material in the scene induced by illumination, shadowing, weathering and other environmental effects. The method offers advantages in multi-spectral data sets where the limited number of channels impairs material un-mixing by standard techniques. The method can also be applied to compress hyper-spectral data. The fractional abundance matrices are sparse and offer an additional compression capability over standard matrix factorization techniques. A description of the method and applications to real and synthetic hyper-spectral and multi-spectral data sets will be presented.

Keywords: hyper-spectral, multi-spectral, end-member, un-mixing, convex cone

1. INTRODUCTION

A goal of analysis of hyper-spectral and multi-spectral imagery is the identification of the materials and objects in the field of view based on the spectroscopic and spatial information contained in the data. Typical scenes may contain many materials and each material will have spectral variability. Even when data has been atmospherically corrected, environmental and illumination effects still persist in the data and more than one spectrum is typically required to describe a material. The number of materials and their spectral variations may exceed the rank of the data sets, the number of linearly independent channels.

The standard linear mixing model is based on a set of material spectra or end-member spectra chosen to model the scene. Each pixel is modeled using the set as a basis. The basis must be linearly independent and its dimension is dictated by the rank of the end-member spectra rather than the number of materials and spectral variations that are present in the data. This limitation leads to poor estimates of material abundances when a basis is inadequate to represent the material and its spectral variations.

While a scene may contain many materials, individual pixels and their immediate surrounds typically contain only a few. This suggests that a collection of local models, each describing a small number of materials and their environmental variations, would provide the desired description of a scene. Strategies have recently been developed for determining abundances when a set or bundle of spectra is used to describe each material. These include a linear programming technique¹ and a regularized constrained least squares approach². Alternatively, stepwise constrained least squares approaches can be used to select subsets of end-member spectra to model each pixel spectra^{3,4}. These linear programming and least squares procedures require an adequate set of end-member spectra that describes the scene materials and their spectral variability.

We have developed convex factorization techniques that can automatically generate the sets of end-member spectra for hyper-spectral and multi-spectral imagery. The end-member abundances are determined simultaneously with end-

^{*}john@spectral.com; phone 781 273-4770; fax 781 270-1161; <http://www.spectral.com>; Spectral Sciences, Inc., 99 South Bedford Street, Burlington, MA, USA 01803-5169.

member extraction via two optimization algorithms, a minimum residual (MinR) and a maximum sparseness (MaxS) algorithm. The MinR optimization has been implemented in SMACC^{2,5}, the Sequential Maximum Angle Convex Cone code. The MaxS algorithm tries to represent each pixel with the minimum number of end-members. Both determine and update abundances simultaneously with finding end-members, avoiding the need for subsequent time consuming and ill-conditioned constrained least squares procedures. A key advantage of the convex factorization techniques is that the number of end-members selected is not limited by the rank of the data or the number of spectral channels. This capability leads to an accurate representation of hyper-spectral data and to an important spatial feature extraction role in multi-spectral imagery data. The end-members selected by convex factorization are the extreme vectors of the convex cone of the data. These are the most unique vectors within the data. The convex factorization leads to sparse abundance matrices with pixels of similar scene materials being described by the same subsets of the end-members. Each subset forms its own convex span, leading to a description of hyper-spectral or multi-spectral data in terms of a set of convex cones one for each material and mix of materials. The overall geometric description of the data is that of a convex polyhedron or polytope.

A second advantage to convex factorization results from the sparseness of the resulting abundance matrices. Convex factorization can lead to higher compression of data over standard factorization techniques, in spite of the larger number of basis functions required for equivalent residual errors of approximation.

A description of the matrix factorization techniques is given in section 2. Section 3 contains a comparison of the method with standard autonomous end-member algorithms using a AVIRIS Cuprite Nevada scene. Also in section 3 is an illustration of the compression capabilities of the technique. The method was applied to the moderately complex AVIRIS scene of the Harrisburg Pennsylvania airport. Finally the capabilities for end-member and abundance map extraction in multi-spectral scenes are illustrated using six visible and near IR LANDSAT channels of a synthetic LANDSAT scene of the Harrisburg airport as an example.

2. METHOD

Matrix factorization techniques can be applied to hyper-spectral data to select unique pixel spectra or to select unique bands. Hyper-spectral data can be given a (row, column) matrix representation, $H(i,j)$, by assigning the N scene pixel spectra to columns and K spectral channels to matrix rows. The data can then be represented by a linear column and/or row expansion.

The expansion in terms of the columns leads to

$$H(i, j) = \sum_k^M S(i, k)F(k, j) + R_s(i, j) \quad (1)$$

where M is the expansion length. The matrix S contains as columns the spectra selected as end-members to represent the data, and the matrix F contains the fractional contribution of each end-spectrum to each pixel. The matrix $R_s(i, j)$ is the error or residual matrix resulting from truncation of the expansion ($M < N$). Note that if the end-member spectra are pixel spectra drawn from the data, F can be thought of as an inventory of the abundance of materials present in each end-member within a pixel.

The expansion in terms of rows, leads to

$$H(i, j) = \sum_l^L C(i, l) Im(l, j) + R_c(i, j) \quad (2)$$

where L is the expansion length. The matrix Im is a matrix of single-channel images of H at channels selected as end-members (end-images) and the matrix C contains the expansion coefficients, the contributions of the L end-images to each data image. Again, $R_c(i,j)$ is the error due to truncation ($L < K$).

For purposes of data compression, it is useful to perform a combined expansion. The combined expansion leads to

$$H(i, j) = \sum_l^L \sum_k^M C(i, l) H_m(l, k) F(k, j) + R(i, j) \quad (3)$$

The matrix H_m is a “mini-cube,” an $L \times M$ matrix of end-members (end-images \times end-spectra). The coefficient matrices C and F retain the same meaning. While the equations are standard linear relations, there are many possibilities for the explicit selection of vectors for S , F , C and Im . Eigenvector analysis of either the autocorrelation matrix or the covariance matrix leads to rapidly converging expansions. Convex analysis leads to sparse coefficient matrices and make expansions in extreme vectors an attractive alternative not only for purposes of interpretation but also for increased compression ratios for equal levels of distortion.

For example, the commonly used principal components analysis performs a row factorization of the data matrix. The channel images are rotated into eigen images, using the eigenvectors Φ of the channel covariance matrix Σ as the channel image coefficient matrix C . In diagonalizing the covariance matrix, the eigenvectors are ordered by eigenvalue λ with the largest eigenvalue, eigenvector pairs being selected for use.

The covariance matrix is given by

$$\Sigma = E\{(h - \bar{h})(h - \bar{h})^T\} = \Phi \lambda \Phi^T \quad (4)$$

where h and \bar{h} represent individual pixel spectra and the mean pixel spectrum, and E is the expectation operator, that is estimated by the average over the entire data cube.

The eigen images are determined by

$$Im = \Phi^T H. \quad (5)$$

Errors in the estimated truncation of the covariance matrix can be determined from the ordered set of eigenvalues with the mean square error, D , and relative mean square error, R , between the original and the approximation using L of the N eigenvector, eigenvalue pairs being given by

$$D = \sum_{j=L+1}^N \lambda_j \quad \text{and} \quad R = D / \sum_{j=1}^N \lambda_j \quad \text{respectively.} \quad (6)$$

The reduction is optimal in terms of expansion length. It has the smallest residual errors for a given expansion length. The technique is effective for compression of channels, typically reducing a hyper-spectral image to 10-20 eigenvectors⁶.

Compression ratio for matrix factorizations

The formula for the compression ratio, CR , based on factorization can be expressed as $CR = \frac{K * N}{M(K + F * N)}$ for pixel

spectra and $CR = \frac{K * N}{L(C * K + N)}$ for channel factorization.

For most hyper-spectral data sets the number of pixels far exceeds the number of channels. When the number of pixels

is very large compared to the number of channels, the compression ratio simplifies to $CR = \frac{K}{M * F}$ for pixel end-

spectra and $CR = \frac{K}{L}$ for channel factorization.

Thus we see for channels, the most efficient representation in terms of basis size, L , will lead to the best compression while the smallest product of basis size and fraction of non-zeros leads to the highest compression ratio for pixel spectra. For non-convex factorization methods, the abundance array is not sparse and the compression ratio is simply the ratio of the number of channels to the number of basis functions. The maximum compression ratio results occur when only one basis or end-member is chosen and equals the number of channels. For a full rank data set, the lower limit of $CR=1$, occurs for non-convex methods when the size of the basis is equal to the number of channels. Compression from non-convex methods occurs when the data can be approximated by reduced rank approximations.

For convex methods, the fraction of non-zero abundances gradually decreases as the number of end-members increases, as more and more of the data is described by blends of only a few end-members. The number of end-members can far exceed the number of channels and still lead to a substantial compression ratio. This will be illustrated in section 3 for an AVIRIS Harrisburg airport Scene.

It should be noted, however, that the compression ratio quoted here ignores any overhead required in the storage of sparse matrices.

Convex factorization algorithms

Two convex factorization (CF) algorithms, MinR and MaxS, have been developed for the sequential factorization of hyper-spectral and multi-spectral data. In addition a Modified Gram Schmidt (MGS) factorization was implemented. The objective of these algorithms is to define the end-members and expansion coefficients of the data matrix. Since the procedure is mathematically the same in either row or column processing, we refer to both end-spectra and end-images as extreme vectors.

There are two steps to each cycle of the sequential factorization algorithms. The first step selects the vector to be added to the current basis or convex span. The second step is the removal of the projection of the currently chosen vector from all of the remaining data vectors.

The currently implemented selection step is the same for all factorization techniques. The criterion used to determine the next extreme vector is its length. Length is the distance that the vector lies outside the sub-space defined by the current basis in the MGS algorithm, or outside the convex span of the current convex cone for the CF algorithms. The first vector is chosen arbitrarily, typical choices are the vector of largest magnitude or the vector least like the average.

The primary difference among the algorithms is the projection step, although the different projections ultimately lead to different vectors being selected in subsequent steps. In the MGS implementation, the selected vectors form a highly linearly independent basis. In sequence, the vectors selected are those that are least like those currently chosen. The MGS method can determine the rank of the data. In the CF methods, the vectors are extreme points of the convex cone of the data. The extreme vectors are not necessarily linearly independent and they can form a over-complete basis.

In the MGS algorithm, the projection is an orthogonal or perpendicular projection. The orthogonal projection leads to the minimum in residual. The convex factorization methods use oblique projections. The two convex factorization algorithms, the minimum residual, (MinR), and the maximum sparseness, (MaxS), technique are based on different optimizations.

The MinR convex projection will be as close as possible to the orthogonal projection while maintaining the positive abundance constraints. It differs from the orthogonal projection only when a constraint is active. An active constraint leads to the current vector or one of the previous extreme vectors being removed from the expansion. If no constraints are active, the orthogonal projection is used and the new extreme vector is added to the description of the data vector with no prior one being removed. MinR is analogous to a step wise constrained least squares algorithm, although the active basis is in general different for the individual data vectors; extreme vectors are added and removed from the data vectors independently. The resulting expansion coefficients are equivalent to the coefficients of a constrained least squares calculation, with a subset of the selected basis used to model each pixel spectra.

The maximum sparseness, (MaxS), algorithm attempts to model each data vector with as few extreme vectors as possible. In the MinR technique, the convex projection differs from the orthogonal projection only when a constraint is active, and a smaller projection is required to keep all abundances equal to or greater than zero. In contrast, the MaxS algorithm places emphasis on increasing the sparseness of the coefficient array and seeks projections that will remove prior extreme vectors. The algorithm maximizes the number of zero abundances subject to the positivity constraints and a monotonic decrease in residuals.

The MaxS algorithm differs from the MinR technique only when no constraints are active, and MinR would add the new extreme vector to the current description. In the maximum sparseness algorithm, whenever the orthogonal projection does not activate constraints, a larger oblique projection is sought that will cause a prior extreme vector to be removed. If no prior extreme vector can be replaced with a simultaneous reduction in residual, the orthogonal projection is used. The different projections are illustrated in Figure 1. The length of the vertical is the residual norm for the orthogonal projection. The lengths of the oblique rays are the residual norms for the MinR and MaxS oblique projections, respectively. To have a reduction in residual, the length of the oblique rays must be shorter than the length of the prior residual of the i^{th} data vector, \vec{r}_i .

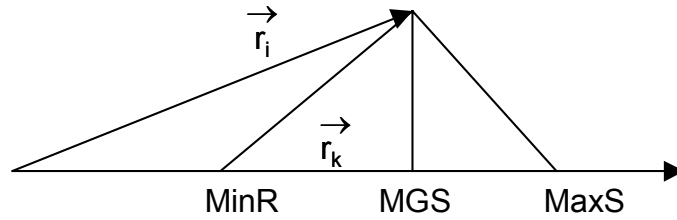


Figure 1. Orthogonal projection of the modified Gram Schmidt, (MGS), factorization and the oblique projections of the minimum residual, (MinR), and maximum sparseness, (MaxS), convex factorizations.

Fractional abundances

The projection coefficients satisfy inequality constraints that ensure that the end-member spectra are added positively, but their sum is not restricted. With the sum to one constraint not applied, the convex basis forms a convex cone rather than a convex hull. The additional degree of freedom leads to a better fit to pixel spectra and avoids the need to form simplices during the processing. In the convex cone approximation, the interpretation of the coefficients can be made in terms of fractional contributions to the total radiance or reflectance. Summing the channel radiances in the mixed pixel

$$\sum_A I_A f_A = I_{\text{Pixel}}$$

and end-member spectra leads to $f_A = I_A / I_{\text{Pixel}}$, where I_{Pixel} is the sum of the channel radiances in the pixel and I_A is the sum of the channel radiances in the A^{th} end-member spectrum. The equality is in the least squares sense assuming that the channel residuals sum to zero. The fractional contribution of radiance from end-member A to the pixel radiance is, the quantity $I_A f_A / I_{\text{Pixel}}$. Note that this relation holds regardless of whether the sum to one constraint is applied and active. To obtain an estimate of the pixel fill or material abundance in the pixel, it is necessary to address the variability in material spectra that exists in the scene. We include the variability in the material spectra by the inclusion of an end-member basis for each material.

3. APPLICATIONS

In this section three applications of the methods are described. First, the models are compared with other autonomous end-member algorithms and applied to the AVIRIS Cuprite Nevada scene for comparison. AVIRIS is a hyper-spectral sensor with 224 spectral channels from 0.4 μm to 2.5 μm . The second application is to a AVIRIS scene of the Harrisburg Pennsylvania airport. In this application, the compression capabilities of the MGS and convex factorization techniques are compared. Finally a synthetic LANDSAT scene derived from the AVIRIS Harrisburg airport, was processed to illustrate the capabilities of the convex techniques for multi-spectral imagery.

Three autonomous end-member algorithms were compared recently by Michael and Edwin Winter⁷. These include ORASIS⁸, N-FINDR⁹ and Iterative Error Analysis (IEA)¹⁰. These were also compared to the interactive pixel purity index method¹¹. All were applied to the AVIRIS Cuprite Nevada scene and the results were found to be similar for all of the methods.

ORASIS is a suite of codes that can find end-members from a scene autonomously. It uses a Modified Gram-Schmidt algorithm to factor the data matrix, followed by a shrink wrapping technique to find an outer simplex^{12,13}. After the end-members have been found, a constrained linear mixing model can be used to obtain material abundance maps. Alternatively, to maintain speed for real time processing, ORASIS has the option of skipping the shrink-wrapping, using the vectors selected by the modified Gram Schmidt procedure and a set of filter vectors¹⁴ derived from unconstrained least squares. The “abundances” are not sparse as a consequence of using filter vectors and any resulting compression comes from the convergence of the expansion.

N-FINDR is an end-member code that runs autonomously and finds pure pixels that can be used to describe the mixed pixels in the scene. The algorithm “inflates” a simplex within the data and selects the largest volume simplex. The end-member determination step of N-FINDR is fast, but like ORASIS, a constrained linear mixing model is required to obtain abundances, a time consuming step. It has been estimated⁷ that the constrained un-mixing takes four times longer than the unconstrained least squares un-mixing.

The Iterative Error Analysis (IEA) approach performs a sequence of constrained un-mixings, starting with the data point (spectrum) that is least well modeled by the average and selecting additional end-members from the poorest modeled data points at each step. The method finds extreme points in the data to use as end-members. At each step a simplex is formed from the selected data points. The process terminates when the number of end-members sought are found or a selected tolerance on residual error has been met.

Our MGS method is similar to the ORASIS mode when shrink-wrapping is not applied. The first several end-members selected by the minimum residual factorization algorithm and the maximum sparseness algorithm will resemble those obtained by single simplex techniques. The distinctions between single simplex methods and the extreme vector approach are illustrated in Figure 2. Outer simplex methods find points outside the data array while inner simplex methods seek to use data points. When selecting fewer end-members than the rank of the data, all of the techniques seek linearly independent vectors. The similarity was confirmed by our processing of the Cuprite scene.

The Cuprite site has been the focus of several AVIRIS measurement campaigns and the collected data has been subjected to much analysis. The site is a mining area in southern Nevada and has little vegetation. The data that was used in this work contains 50 of the spectral channels 1.991 μm to 2.479 μm of ATREM corrected reflectances. The data is supplied as sample data with ENVI. The three major materials present are alunite, kaolinite and calcite. The Cuprite scene was processed with both the MGS and convex cone factorization approaches. The three most abundant spectra found by the factorization techniques are similar in shape to the laboratory spectra of alunite, kaolinite and calcite and strongly resemble end-members extracted by other techniques⁷. The magnitude of the laboratory reflectance spectra depend on particle size¹⁵, while atmospheric correction artifacts affect the magnitude as well as details in shape of the AVIRIS measurements. N-FINDR and our approach find actual pixel spectra in the data, while the ORASIS and IEA end-members are scaled. The first six end-members found by the MGS and convex cone factorization techniques were the same. These extracted end-members are plotted in Figure 4a and Figure 4b. Once constraints become active, departures from the MGS and convex methods are expected. Some extreme points in the data can be modeled to within the desired tolerance by the unconstrained basis set and they are not selected by the MGS method.

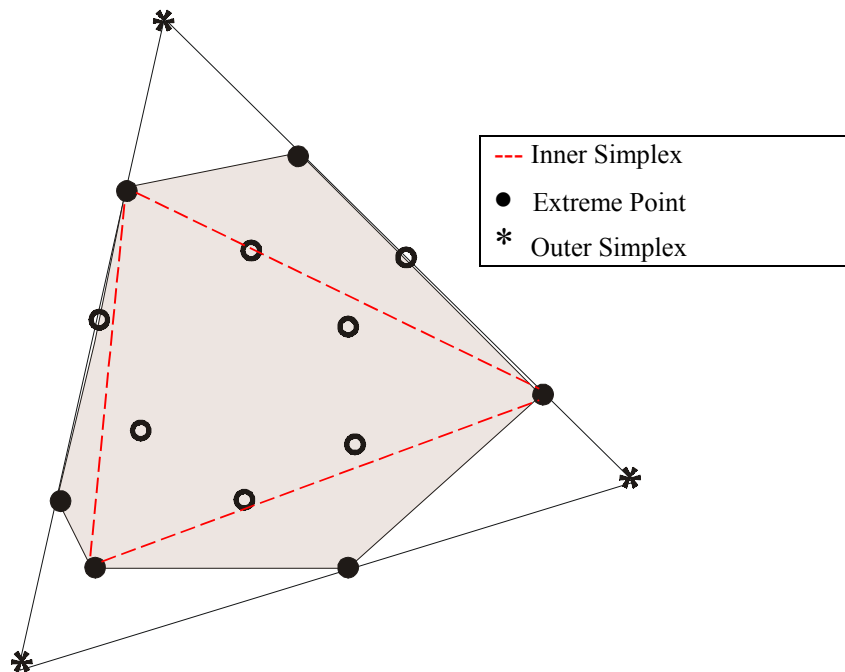


Figure 2. Comparison of simplex and extreme point end-member methods projected onto a plane. The shaded area is the convex hull of the data. The solid circle points are data extrema identified by the convex factorization as end-spectra. The star points are outer simplex end-spectra. The dash line triangle outlines the hull of an inner simplex formed from data points. Note that no inner simplex can completely describe the data, and no outer simplex can be formed from data points alone. The interior (e.g., open circle) points are mixed pixels.

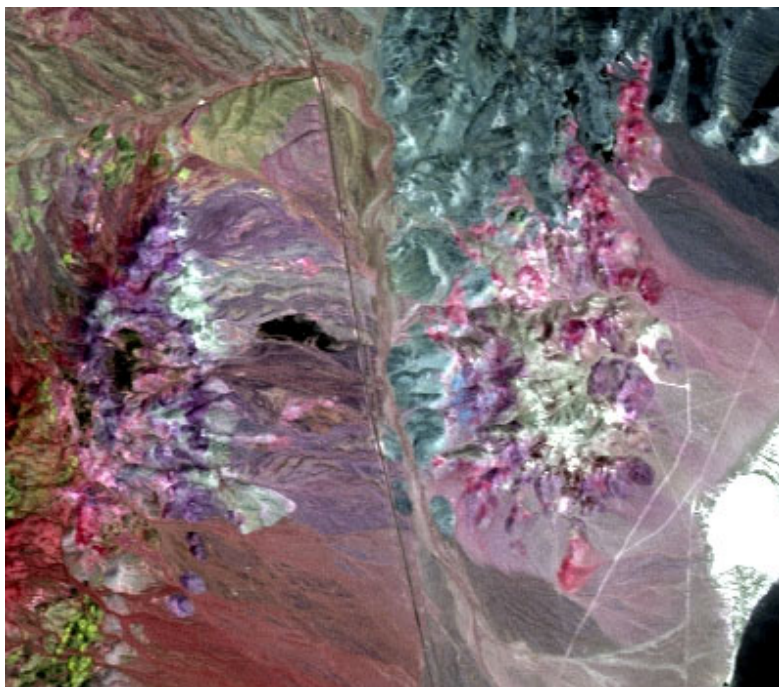


Figure 3. Composite image of the Cuprite Nevada Site.

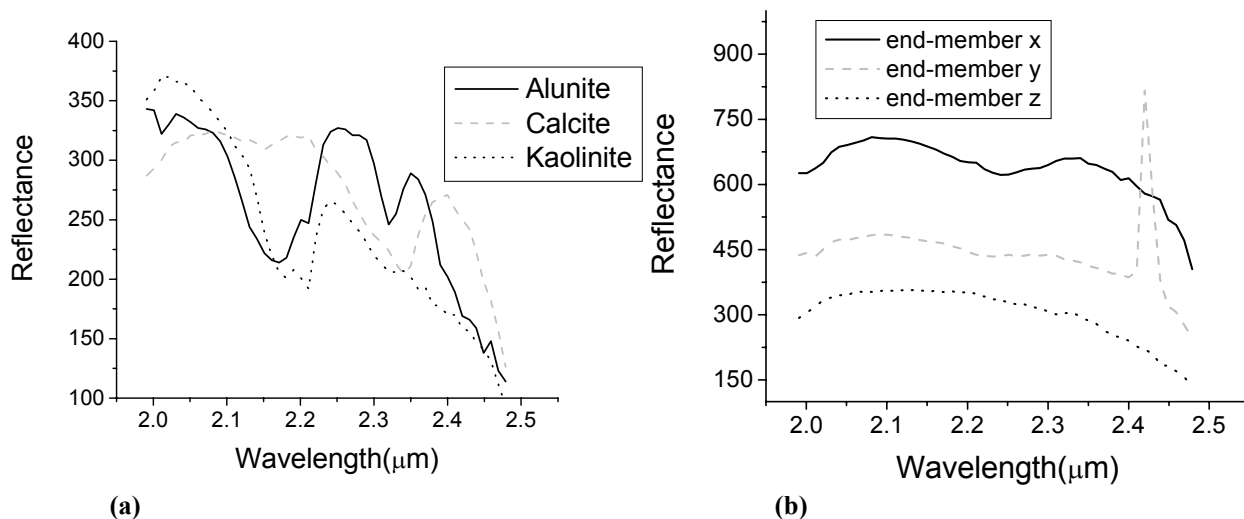


Figure 4. (a) The three major component end-member spectra extracted from the AVIRIS Cuprite Scene. (b) Three additional end-member spectra common to both the MGS and CF methods.

AVIRIS Harrisburg airport scene

An AVIRIS Harrisburg airport data set was selected as a test case for a data compression study. An image is shown in Figure 5. The scene is a 401x401 pixel array. The data set contains all of the 224 AVIRIS spectral channels from 0.4 μm to 2.5 μm . We used the data directly with no atmospheric correction. We studied the compression characteristics of our CF method and our MGS method as a function of the number of end-members or basis functions. The compression ratio (CR) is defined in section 2. Increasing the number of end-members used to describe a dataset improves the fidelity of the data but also the amount of information that must be stored. The compression ratios for both decrease monotonically, but the behavior is quite different for the two methods. The MGS compression ratio is governed by the number of channels divided by the number of basis functions. The convex factorization method maintains high compression ratios as the number of end-members increases. The comparison is illustrated in Figure 6a. At 40 end-members the maximum sparseness CF compression ratio is 51/1, the minimum residual CF compression ratio is 35/1. The MGS compression ratio for 40 basis functions is reduced to less than 6/1 and is 28/1 at 8 basis functions. However the unconstrained perpendicular projections of the MGS technique reduce the residual errors at a much faster rate. A comparison of the spectral errors of the MGS and minimum residual CF method for compression ratios of 28/1 and 35/1 are given in Figure 6b. We have plotted the average error for all pixels, as well as the pixel with maximum error. The average pixel spectrum from the scene is included for signal level comparison. The magnitudes of the average errors are similar for the CF and MGS methods. The convex factorization does better at reducing the maximum magnitude of errors for a given level of compression ratio. The convex factorization contains many more vectors at a given compression ratio, and these vectors account for the reduction in outlier spectral features. Real advantages to using the extreme vectors rather than an MGS basis will depend on efficient compression algorithms for the sparse abundance matrices. The effort requires further investigation.



Figure 5. Composite of AVIRIS Harrisburg airport scene

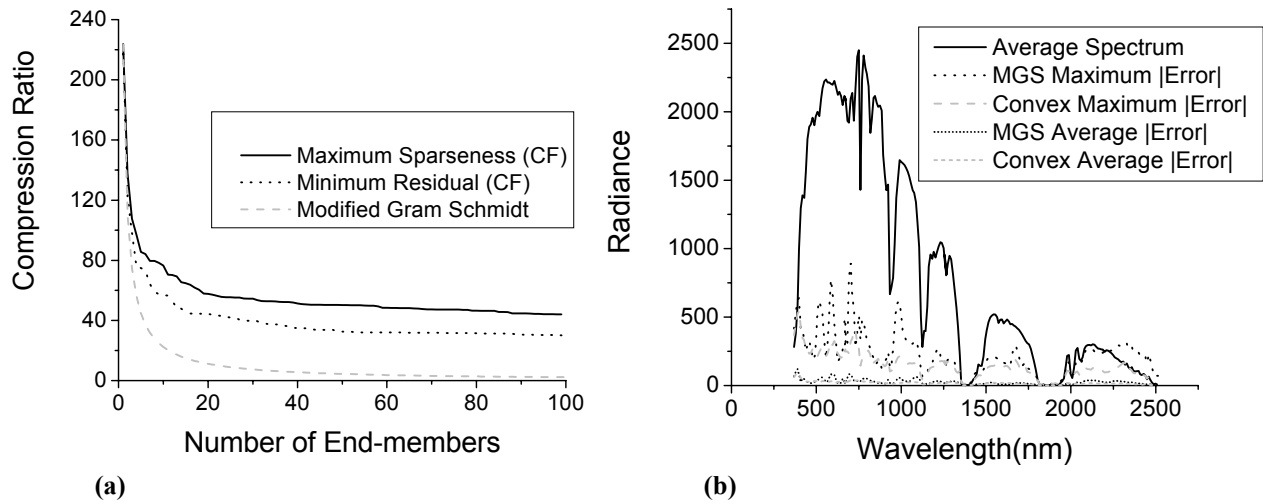
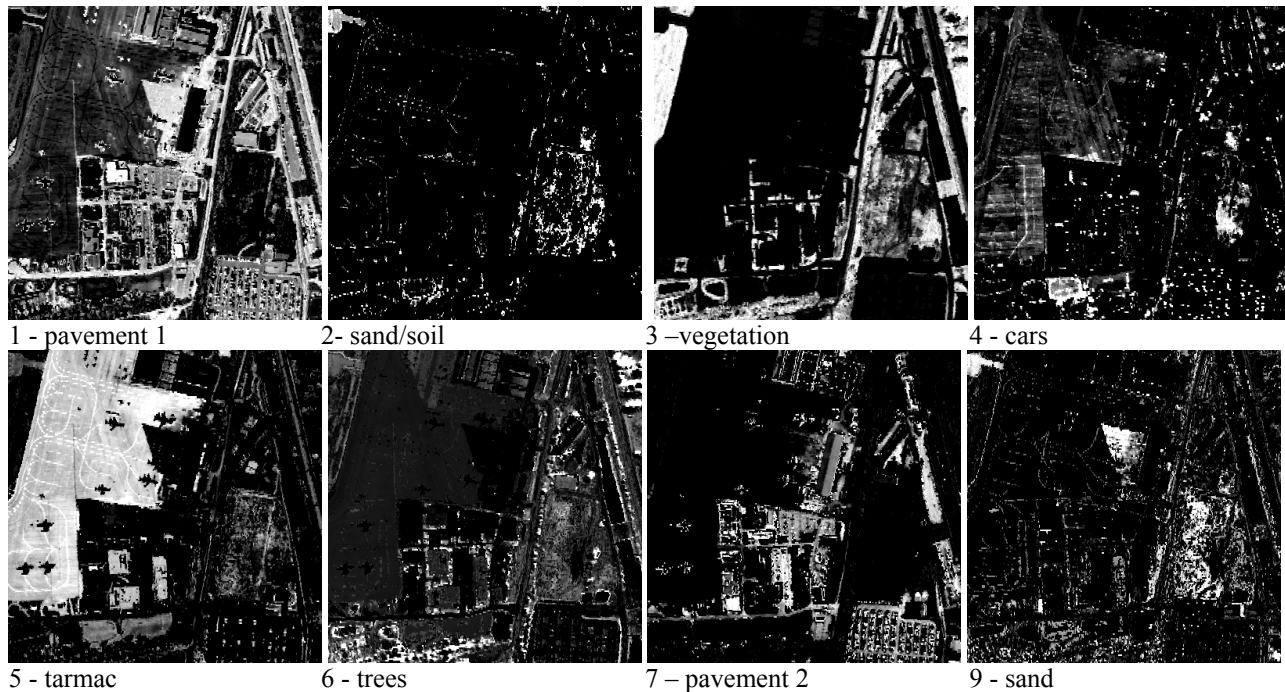


Figure 6. (a) Compression ratio achieved for convex factorizations (CF) and Modified Gram Schmidt factorization of the Harrisburg airport scene. (b) Errors due to compression using the minimum residual factorization CR=35/1 and Modified Gram-Schmidt CR=28/1 on the Harrisburg airport scene.

Multi-spectral application

We illustrate this capability using the AVIRIS Harrisburg Airport scene discussed above. The spectral resolution was reduced to the six visible NIR LANDSAT channels to simulate LANDSAT data. The CF algorithm was applied to the multi-spectral data and fifty end-members were found. The abundance maps for 11 of the first 16 end-members are shown in Figure 7. The algorithm found several more unique features within the data than the six channels would imply. In comparison with the results for the six channel data versus the 224 channel full data set, it was found that while the end-members were chosen in a different order, 18 of the first 20 unique pixel spectra selected as end-members of the full data set were also selected from the simulated LANDSET data. The same pixels were chosen as the most unique.



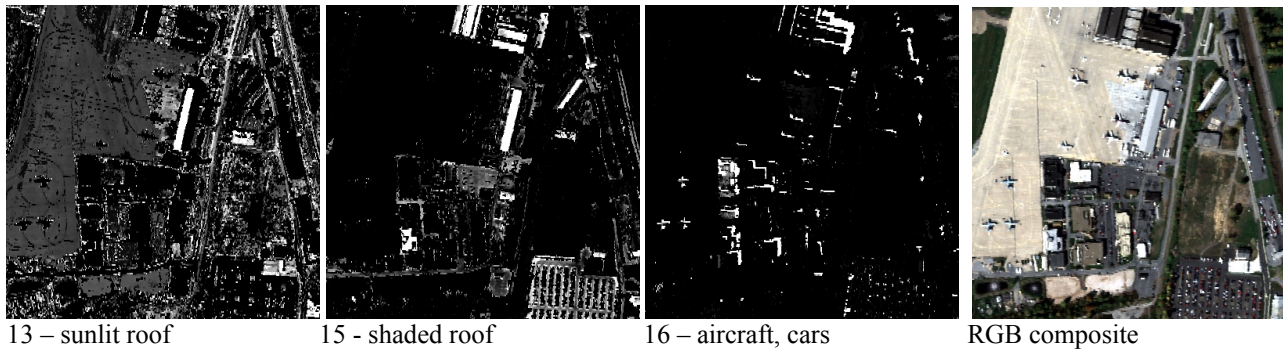


Figure 7. Spatial Details contained in 11 of the first 16 end-members selected by CF for the 6 channel synthetic LANDSAT image of the Harrisburg airport

4. CONCLUSIONS

Our CF approach provides a physical model for hyper-spectral and multi-spectral imagery data. Materials and their spectral variations induced by environmental and illumination variations are modeled with scene spectra that are extracted as end-members. The approach leads to multiple mixing models with subsets of the end-members representing the materials in the scene. Both end-members and abundances are determined simultaneously and autonomously. The method provides a unique processing capability for multi-spectral data. It is not limited by the number of channels and can extract the spatial and spectral description of several more materials than the number of channels. Geometrically the over-completeness of the extracted basis sets is a result of the direct use of extreme points as illustrated in Figure 2.

5. ACKNOWLEDGEMENTS

This work was generously supported by Spectral Sciences, Inc. Work on image compression aspects of the factorization was supported by a NASA SBIR NAS5-01217. We also acknowledge AFRL/SN and AFRL/VS for support for preliminary development of SMACC.

6. REFERENCES

1. C. Ann Bateson, Gregory P. Asner, and Carol A. Wessman, "End-member Bundles: A New Approach to Incorporating End-member Variability into Spectral Mixture Analysis", *IEEE Transactions on Geosci. and Remote Sensing*, **38**, 1083-1094, (2000).
2. J. Gruninger, M.J. Fox and R.L Sundberg, "Hyper-spectral Mixture Analysis Using Constrained Projections onto Material Subspaces", *Proceedings International Symposium on Spectral Sensing Research (ISSSR) Quebec City*, pp 162-170, June 11-15 (2000).
3. Fabio Maselli "Multiclass Spectral decomposition of remotely Sensed Scenes by Selective Pixel Unmixing", *IEEE Transactions on Geoscience and Remote Sensing*, **36**, pp1809-1820,(1998).
4. Gary D. Robinson, Harry N. Gross and John R. Schott, "Evaluation of Two applications of Spectral Mixing Models to Image Fusion", *Remote Sens. Environ.* **71**, 272-281 (2000).
5. J. Gruninger, R. L. Sundberg, M. J. Fox, R. Levine, W. F. Mundkowsky, M. S. Salisbury and A. H. Ratcliff, "Automated Optimal Channel Selection for Spectral Imaging Sensors", *Proceedings SPIE 4381*, Algorithms for Multi-spectral and Hyper-spectral Imagery VII,[4381-07], Orlando April (2001).
6. Su May Hsu, Hsiao-hua Burke and Michael Griffin, "Adaptive HSI Data Processing for Near-Real-Time Analysis and Spectral Recovery" *Proceedings of the Tenth JPL Airborne Earth Science Workshop*, NASA Jet Propulsion Laboratory, California Institute of Technology Pasadena California (2001).
7. Michael E. Winter and Edwin M. Winter, "Comparison of Approaches for Determining End-members in Hyper-spectral Data" *Proc. IEEE Aerospace Conference*, Big Sky Montana, March 18-25 (2000).
8. J. Bowles, M. Daniel, J. Grossman, J. Antoniadis, M. Baumbach and P. Palmadesso, "Comparison of Output from ORASIS and Pixel Purity Calculations", *Proc. SPIE Imaging Spectroscopy IV*, **3438**, pp 148-156, San Diego July 19-24 (1998).

9. Michael E. Winter, "N-FINDR: An Algorithm for Fast Autonomous Spectral End-member Determination in Hyper-spectral Data" *Proc. SPIE Imaging Spectroscopy V*, Vol. **3753**, 266-275, Denver July (1999).
10. R. A. Neville, K. Staenz, T. Szeredi, J. Lefebvre, and P. Hauff, "Automatic End-member Extraction from Hyper-spectral Data for Mineral Exploration", *Proceedings of the fourth International Airborne Remote Sensing Conference and Exhibition / 21st Canadian Symposium on Remote Sensing*, Vol. II, 891-897, Ottawa, Ontario Canada 21-24 June (1999).
11. Joseph W. Boardman, "Analysis, understanding and Visualization of Hyper-spectral data as Convex Sets in n-space", *Proc SPIE* **2480**, Imaging Spectroscopy pp 14-22, Orlando April (1995)
12. M. D. Craig, "Minimum-Volume Transformations for Remotely Sensed Data", *IEEE Trans. Geoscience and Remote Sensing*, **32**, 99-109, (1994).
13. Daniel R. Fuhrmann, "A Simplex Shrink-wrap algorithm", *Proc. SPIE* **3718** AeroSense ATR IX, 155-166, Orlando April (1999).
14. P. Palmadesso, J. Antoniadis, M. Baumbach, J. Bowles and L. J. Rickard, "Use of Filter Vectors and Fast Convex Set Methods in Hyper-spectral Analysis" *ISSSR*, Australia, November (1995).
15. JPL-library reference spectra with different grain sizes to account for particle size ---C. I. Grove, S. J. Hook, E.D. Paylor II, "Laboratory Reference Spectra of 160 Minerals .4 to 2.4 Micrometers, JPL Publication 92-2, (1992).